Journal of Sustainable Energy & Environment

11 (2020) 43-48

Experimental flow visualization and performance analysis of horizontal water-air ejector system

Muhammad Penta Helios[1,2,*], Wanchai Asvapoositkul[3] and Kyung Chun Kim[4]

[1] The Joint Graduate School of Energy and Environment, King Mongkut's University of Technology Thonburi, Bangkok 10140, Thailand
[2] Center of Excellence on Energy Technology and Environment, Ministry of Higher Education, Science, Research, and Innovation, Bangkok 10140, Thailand
[3] Department of Mechanical Engineering, Faculty of Engineering, King Mongkut's University of Technology Thonburi, Bangkok, 10140, Thailand
[4]School of Mechanical Engineering, Pusan National University, Busan, 609-735, Korea
*Corresponding author: muhammad.helios@mail.kmutt.ac.th

Abstract: This paper presented an experimental study of water-air two-phase flow in the throat-diffuser region of a horizontal ejector. The aims are to visualize flow patterns and to assess the performance of ejector at different backpressure. The performance was described into dimensionless terms, i.e., the pressure ratio and volumetric ratio. The ejector operated at a constant water flow rate and six different back pressure as the operating condition. Both non-intrusive and intrusive methods were applied to visualize the flow and to record related data of performance, i.e., flow rate, pressure, and temperature simultaneously. An image processing algorithm and performance analysis were employed simultaneously to analyze the images, while sensor data recording was used to evaluate the ejector's performance. The results revealed that the two flow patterns appeared with increasing of backpressure, namely the stratified-wavy and bubbly flows. The binary image exposed that the highest performance of the ejector obtained when the bubble generation and mixing process happened at the middle and end section of the throat, respectively. As the mixing process results, the highest area gas fraction and performance increased with increasing backpressure ratio. It indicated intimate air dispersed in water occurs pointed by declining of the volumetric ratio.

Keywords: High-speed camera, stratified-wavy flow, bubbly flow, mixing process, ejector performance.

1. Introduction

The liquid-gas ejector is a gas remover device that is to evacuate, to remove and to transport troublesome gases in the system. It is also used as a static mixer for the intense mixing of two fluids [1]. Due to its favourable mass transfer and mixing characteristics, the liquid-gas ejector is increasingly used in any industries, i.e., chemical, power generation, agriculture, and refrigeration [2]. The complexity behaviours of two-phase flow, i.e., pattern, phenomena, and parameter in a central-driven ejector are still challenging to be understood. There are two general techniques used for flow measurement, namely intrusive and non-intrusive. The intrusive technique allows the instrument's contact to the stream location and affects the flow, while the non-intrusive method locates instruments outside of stream and does not affect the flow.

Numerous experiments have been developed and conducted to study the effects of two-phase flow towards ejector's performance [3-8]. Most of the experiments use intrusive method to achieve data related to performance. The liquid-gas phase ejector's performance is identified by the intimate mixing of both phases, in which the bubbly flow appeared in the throat-exit of the ejector. The phenomena known as mixing shock referred to the optimum mixing process location [3]. At that point, the liquid-jet breakup to be finer droplet and collided with airflow [4]. In the case of existing ejector with low performance, mixing phenomena can be achieved by changing the motive fluids [5], adjusting geometry (spacing and throat-aspect ratio) [6], and operating conditions (mass flow rate and back pressure) [7-8]. However, it has limitations to analyses the relation between the flow behaviour - mixing process and ejector performance using an intrusive method only.

Since rapid development optical and camera technology for fluid measurement applications, high-speed imaging grows into a powerful and promising non-intrusive technique that is essential to record and to visualize flow behaviour images at high spatial, temporal, and optical resolutions. In the present study, synchronizing the flow visualization by digital image processing techniques and performance data of water-air ejector by experimental measurement have been carried out. Since the relation between mixing location and ejector performance under different back pressure is not widely discussed and investigated yet in the scientific viewpoint. It becomes the motivation of this research to achieve better insight into the mixing process to performance.

2. Experimental Setup

2.1 Ejector loop system and flow condition

In this experiment, the ejector dimension from the previous study is adopted [2]. Basic parameters were nozzle diameter of 7 mm, throat diameter of 12.7 mm throat length-diameter ratio of 7, and diffuser angle of 7º. Since flow visualization was the focus of this study, the ejector test section had been modified and fabricated by a transparent material. It consisted five components i.e. 1) nozzle; 2) throat-diffuser; 3) chamber-convergent 4) refractive box and 5) outlet section as shown in Figure 1a. A 150 × 150 ×

150 mm^3 rectangular box as fill-of-view (FOV) filled by water, where the throat-diffuser as region-of-interest (ROI) is longitudinally mounted inside as shown in Figure 1b.

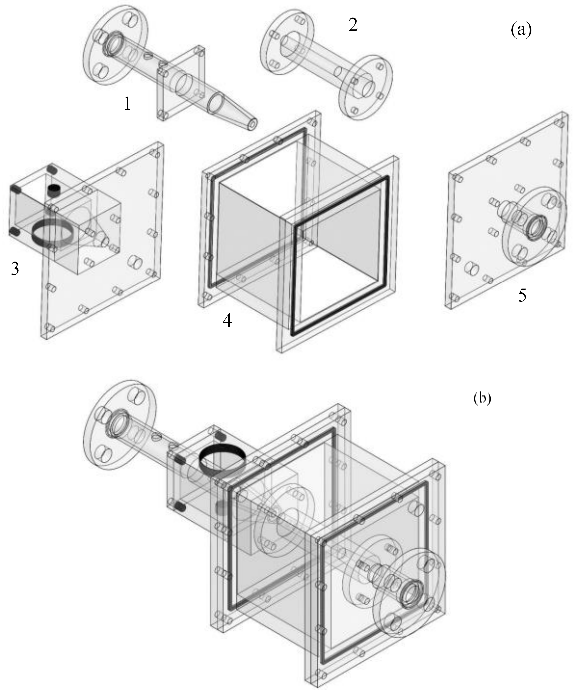

Figure 1. Ejector test section (a) parts and (b) assembly.

In this study, the water was used as a motive fluid to generate a low-pressure region at the nozzle exit. The air as a secondary fluid was entrained into the ejector chamber. The mixing of both fluids occurs in the throat to the end of the diffuser as mixture flow. The constant water flow rate (30 L/min) and six back pressure (0, 4, 8, 12, 16, 20 kPa) were controlled by adjusting the gate valve.

The schematic of an open-loop ejector system shown in Figure 2. A water pump (LG: PU780M) with 15 m head was installed for circulating water. The water flow rate was controlled by ball valves manually and measured by a turbine flow meter (Kometer: KF-550-F series), while a rotameter (Dwyer: RMA-23- SSV) measured the airflow. Three pressure transmitters and three thermocouples were attached in the system to monitor and record the pressure and temperature of both water and air. It was purposed to maintain the isothermal process. The accuracy of water flow meter, airflow meter, pressure transmitter, and thermocouple are 0.5%, 4%, 0.25%, and + 0.75 K, respectively.

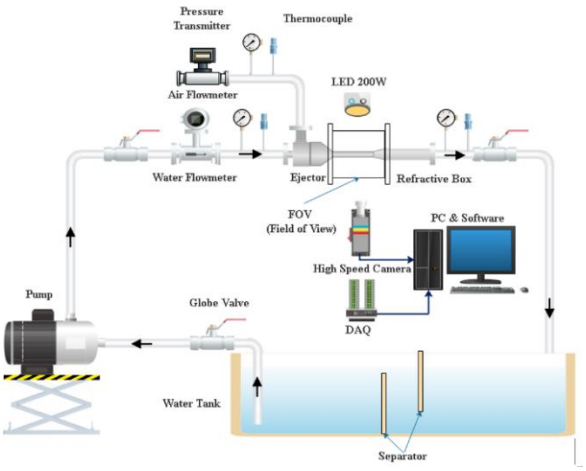

Figure 2. The schematic experiment of the horizontal ejector.

NI 9203 and 9213 modules assembled into a DAQ board (NI 9174) at 1 Hz frequency gathered all sensor signals. The LABVIEW as interface program processed the ensemble signal for each sensor. Later, the performance of the water-air ejector was assessed by using the data collection. Two ratios, i.e., the volumetric ratio (Q^*) and pressure ratio (P^*), are determined by the equation as follows:

$$Q^* = \frac{Q_a}{Q_w} \tag{1}$$

$$P^* = \frac{P_{a,in} \ln\left(\frac{P_{out}}{P_{a,in}}\right)}{(P_{w,in} - P_{a,in})} \tag{2}$$

Where Q and P represent flow rate and pressure respectively, meanwhile subscript *a*, *w*, *in* and *out* stand for air, water, inlet, and outlet. Thus, the ejector's performance (η) equation becomes

$$\eta = Q^* \times P^* \tag{3}$$

2.2 High-speed camera setup and image processing

A high-speed camera (Phantom VEO-410L) with an advanced CMOS sensor was used to capture flow patterns in the field-of-view (FOV). According to fluid flow velocity, this study employed the 6200-fps recording speed and 1024 × 786 spatial resolution. Additional 200W LED lamp (LED200WP) backlighting and 105 mm focal length lens (AF Micro Nikkor) was installed, respectively. Finally, the flow was recorded as video in s with the time interval between two images about 0.149 s. Finally, about 1000 images were selected for image processing.

The analysis of captured images used the image processing algorithm of Fiji software. The detail of this method was discussed in [9-10]. Figure 3 depicts the image processing algorithm of this study. At first, the video was converted to grayscale 8-bit TIFF format images. The grayscale images were imported to the Fiji software. Frequently, the light intensity of the image was not uniform and mostly concentrated in the centre of FOV, so the brightness and contrast adjustment were implemented to achieve uniform grayscale level [11]. Then, the sorting process was conducted for selecting good quality images. Before reduction image resolution due to the unwanted region, image calibration minimized the difference size between image and actual dimensions. Henceforth, the median filtering process was employed to minimize noise later. Inhomogeneous background illuminations are applied to identify each phase by the local threshold using Otsu's method at morphological operation [12]. Each image was converted to black (1) and white (0), in which the black colour represented bubble/air, while white colour was water. However, the uneven background was still existing due to blocking light. The background subtraction was proposed as a proper method to enhance a clear image [13]. Commonly, the easy way was by subtracting with the background image without moving fluid [14]. At that point, the colour representing water and air was inverted after it changes to a binary image. It was purposed and required to find the perimeter of the area covered by the bubbly flow. As a final step, segmentation was implemented to separate the air/bubble area and the background. Since the area of throat-diffuser could be determined from the actual dimension, the area air/bubble fraction was assessed. The area bubble fraction (ε_g) was defined as the total pixel cover by the air bubble (n_j) to the total pixel of the throat-diffuser region (n_r) on the calibrated image. [15]. It can be determined by using the equation as follow:

$$\varepsilon_g = \frac{A_b}{A_{tot}} = \frac{\sum_j n_j}{\sum_r n_r} \tag{4}$$

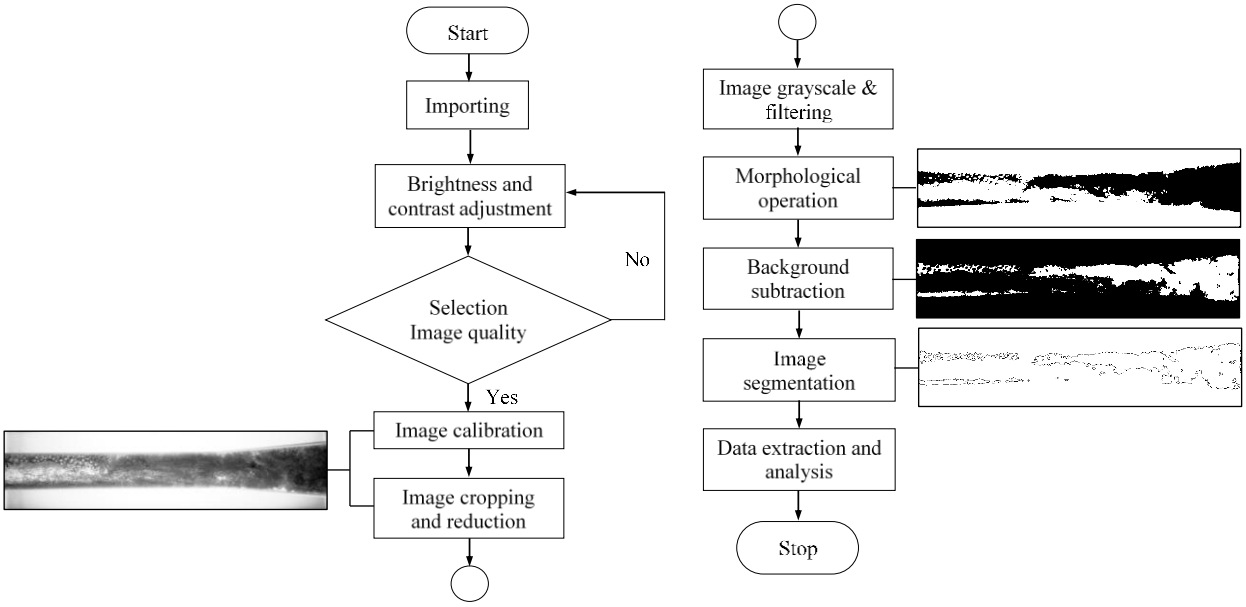

Figure 3. Image processing algorithm.

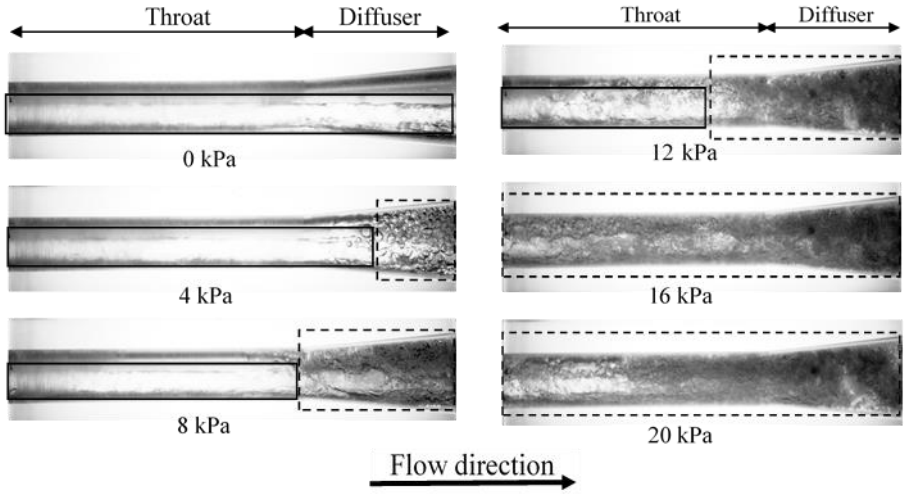

Figure 4. Instantaneous flow patterns, stratified-wavy (solid line) and bubbly (dash line).

3. Results and Discussion

3.1 Flow visualization

The stratified-wavy and bubbly flows are identified as the most frequent flow pattern, as shown in Figure 4. Stratified-wavy flow as a basic flow pattern for two-phase flows fully appears at 0 kPa of backpressure. It can be observed from the water-air interphase, which is wave amplitude from throat entry to diffuser exit. The stratified-wavy flow still exists in the throat when the backpressure rising from 4 to 8 kPa, although the bubbly flow overgrows and moves back into the diffuser. Henceforth, it is seen that the water jet core is bent at the end of throat-exit due to the gravitational field effect.

Differ from the stratified-wavy flow. The bubble swarm generates along the throat with increasing back pressure from 12 to 20 kPa, where the bubble as lighter fluid flows above the heavier ones. Then, high dense of bubble generation completely present along throat-diffuser when the backpressure increases close to critical condition from 16 to 20 kPa. Overcritical condition of backpressure, the ejector becomes malfunction – air flow rate undetected by the rotameter. At this point, the amount of water is reversed to the chamber and blocks the airflow.

3.2 Mixing process identification

Since the field-of-view (FOV) is too large, the resolution and the dimension of the image is reduced by the masking method. The unnecessary region is diminished, and the resolution is reduced to 913 × 215 pixels with corresponding to 110 mm × 25 mm. Fiji software is used to distinguish the area of air/bubble and water in the 2D planar and isometric 3D surface plot via colour level, as shown in Figure 5. 2D planar view (binary image) is represented by black (1) and white (0).

Since this mode has only two colours level, it may lead to misinterpretation of the mixing process, such as an image of back pressure from 0 to 12 kPa. The black colour in the throat-entry top and bottom side is not only represented by air/bubble but also interprets blocking illumination light due to condensing air film layer inside of the throat. The binary image is accurately used when water and air/bubble full-filled whole tube frame, on the other hand, no space as seen at image 16 to 20 kPa in the bottom right.

3D surface plot view provides a better understanding by converting an 8-bit grayscale image to an 8-bit RGB. This model interprets the air/bubble area in a three-dimensional surface based on the colour intensity (0-255). In this case, the LUT (Lookup Tables) spectrum is selected. The rectangular red colour (255) at

the bottom represents ROI, while another red colour (0) is a dense bubble or mixing process. Another intensity embodies bubble generation and shadow. Similar to the binary image, the shadow at image 0 to 12 kPa has also appeared at the throat entry region, but the represented colour of each condition is different. For instance, it can be seen the tendency of blue colour at image 0 kPa in Figure 5 representing the shadow. Then, the area without colour intensity emphasizes that no mixture occurs.

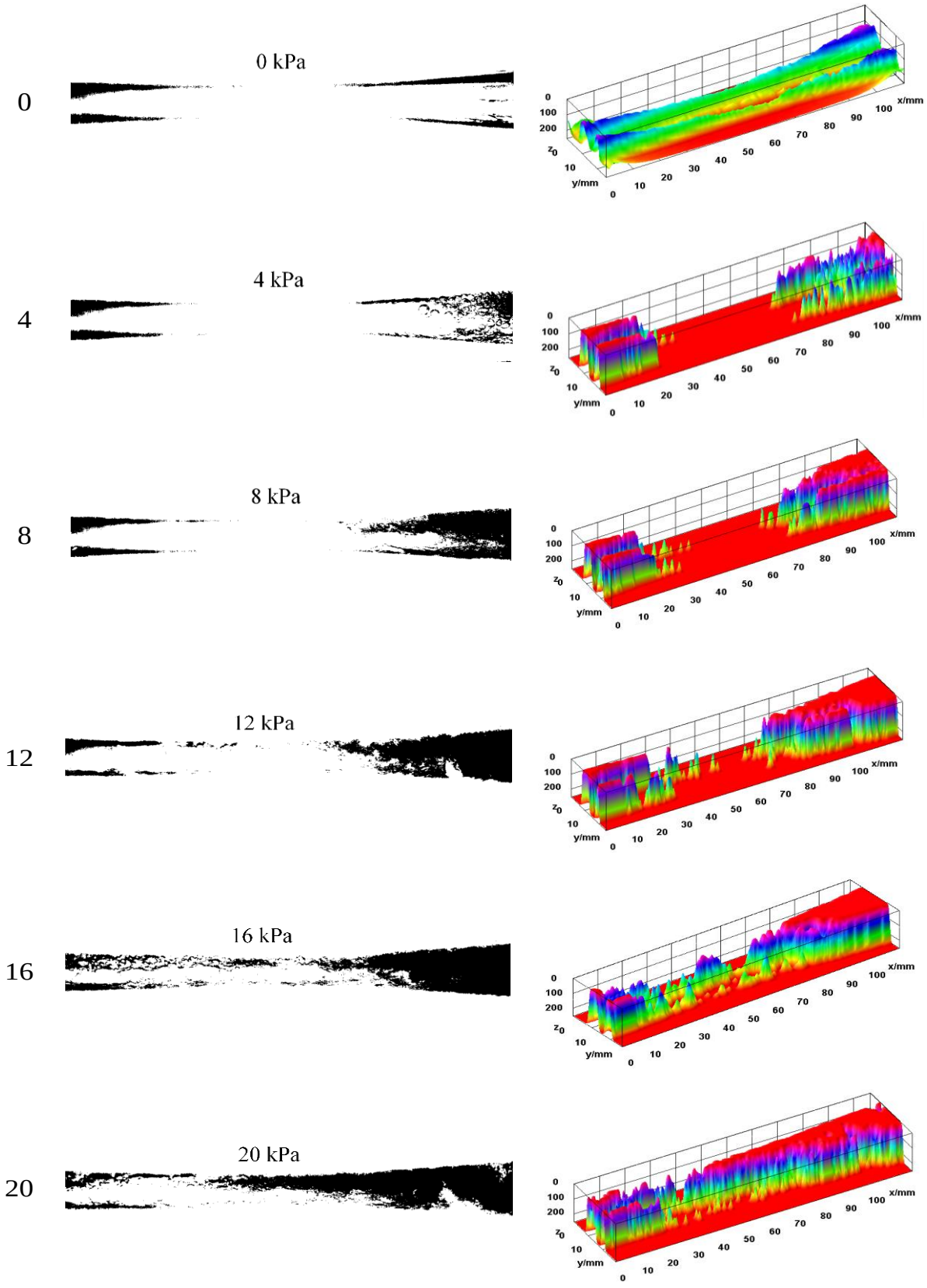

Figure 5. The contour of mixing process under different backpressure; 2D planar (left) and 3D surface plot (right)

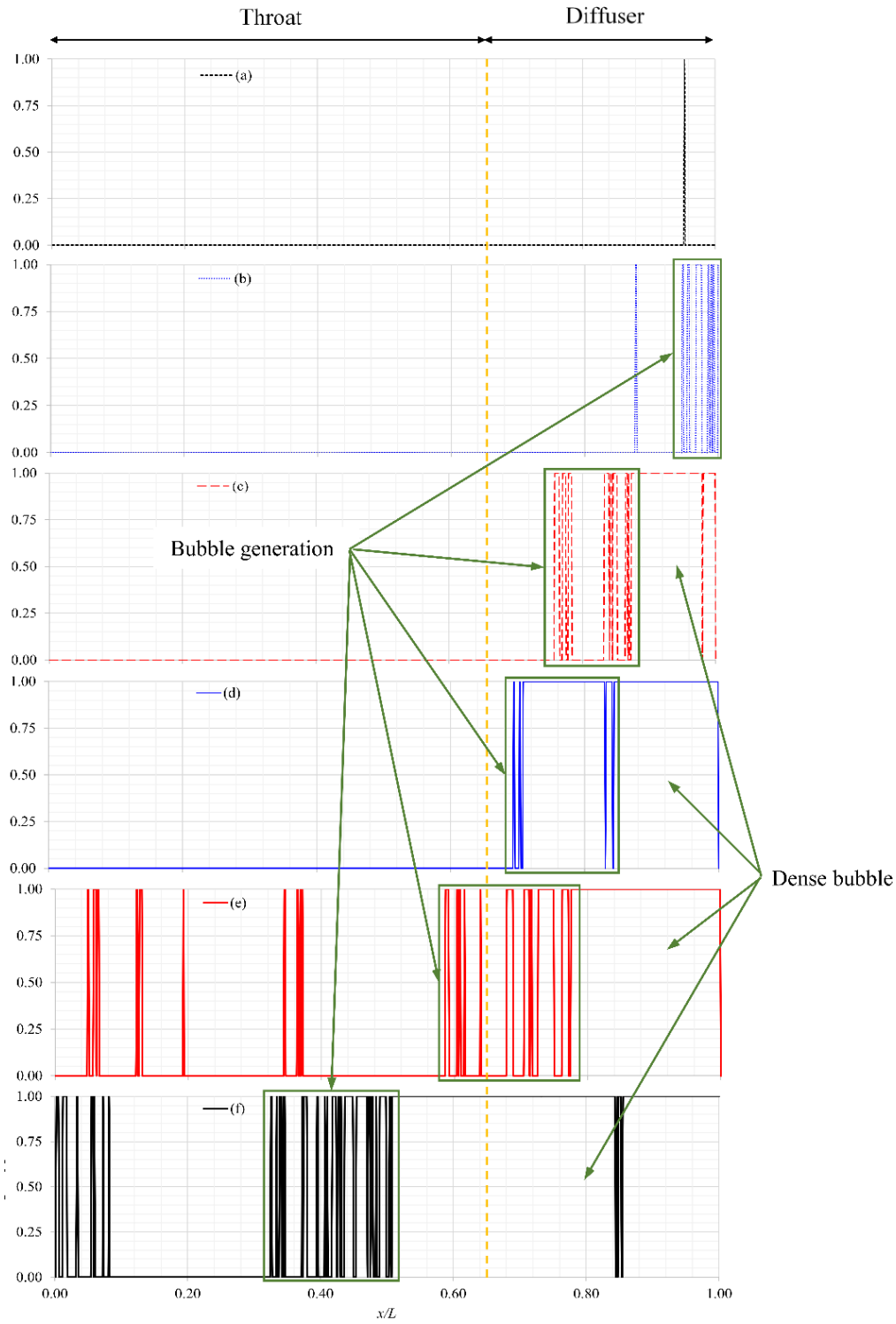

Figure 6. Extraction line of binary image (a) 0 kPa, (b) 4kPa, (c) 8 kPa, (d) 12 kPa, (e) 16 kPa and (f) 20 kPa.

Furthermore, water tends to flow in the centre of the throat-diffuser; therefore, the binary signal of an image can be used for analyzing the mixing process. Figure 6 shows the binary signal extraction of area gas fraction for each case at the centreline of the image. The fluctuation extraction line does not appear in Figure 6a due to a stratified-wavy flow pattern. At that condition, there is no mixture happen since no mixing area exists. The fluctuation line indicates the appearance of bubble generation due to jet break up, as shown in Figure 6b to 6f. Most of the bubble generation present in the throat exit and diffuser region, while other generates bubble in the middle of the throat section (see Figure 6f). Further, the constant value area, as shown in figure 6c to 6f, emphasizes that is air/bubble dispersed due to mixing during increasing backpressure.

3.3 Relation between mixing process and performance

Figure 7 depicts the relation the mixing process represented by area gas fraction to ejector's performance under different backpressure. Figure 7a shows that the area gas fraction increases linearly with an increasing backpressure ratio. Figure 7b the performance tends to increase while the volumetric ratio declines linearly. However, the volumetric ratio is not only a performance

indicator since it also depends on the pressure ratio. Implicitly, the increasing performance reduces the volumetric ratio and increases head ratio as well as area gas fraction.

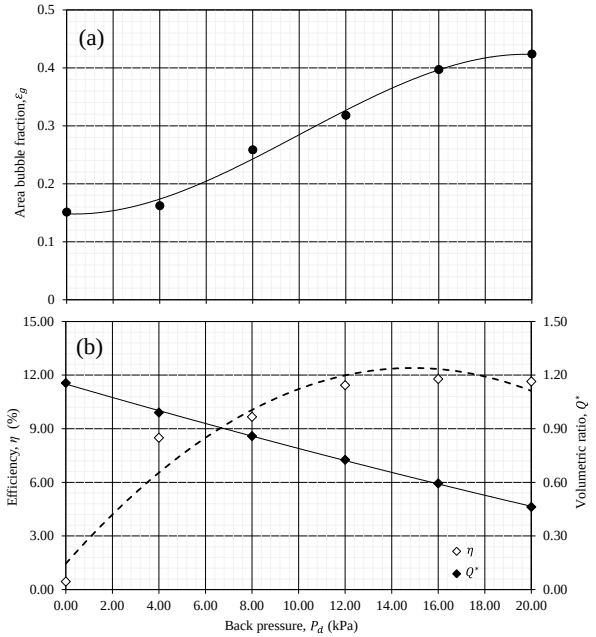

Figure 7. Mixing process and performance relation curve (a) area gas fraction and (b) performance curve.

Also, Figure 7 illustrates information about the optimum operating condition of the ejector. For instance, the ejector operating at 0 area gas fraction evacuates the light fluid without considering gas dispersion into liquid. At this point, the head ratio is the lowest among other points, and the flow pattern is stratified-wavy flow. Further, the ejector transfers the low flow rate of air at ratio 1, indicating the highest head ratio and gas dispersion in the water are achieved (see Figure 7a). At this point, the ejector performance reaches the maximum marked by the bubbly flow with intense mixing happens in the throat exit.

Conclusions

The relationship between the mixing process and ejector's performance has been analyzed by implementing image processing techniques. Quantitative and qualitative data extraction from both measurements, i.e., intrusive and non-intrusive techniques have been used to understand the relation of mixing and performance. From the study, the following conclusions were drawn.

1. The stratified-wavy and bubbly flows were the most frequent flow pattern appear during increasing backpressure. Increasing back pressure forces more rapidly water jet breaks up.
2. The image processing algorithm successfully visualized the area of air/bubble fraction by interpreting images into an 8-bit RGB level due to ability in shadow distinguishing.
3. Extracting line data in the binary image was used. The small digital signal area indicates bubble generation, while the extended digital signal area represents a constant mixing area.
4. The relation between the mixing process and ejector's performance in terms of the backpressure ratio indicated that stratified-wavy flow indicates the low performance of the ejector. The highest performance implied the air well dispersed into the water. At this point, the bubbly flow with intense mixing happens in the throat exit.

Acknowledgement

The authors would like to express their gratitude to Faculty of Engineering, The Petchra Pra Jom Klao PhD scholarship, Grant No. 1/2559, King Mongkut's University of Technology Thonburi, and the Joint Graduate School of Energy and Environment (JGSEE) and the Center of Excellence on Energy Technology and Environment (CEE), PERDO, Ministry of Higher Education, Science, Research and Innovation. This work was partially supported by the National Research Foundation of Korea (NRF) grant funded by the Korean government (MSIP) through the Global Core Research Center for Ships and Offshore Plants (GCRC-SOP, No. 2011-0030013).

References

[1] Cunningham, R.G. 1974. Gas compression with the liquid jet pump, *Journal Fluids Engineering*, 96, 203-215.

[2] Helios, M.P. and Asvapoositkul, W. 2018. *Numerical Investigation of Projection Ratio's Effects on Performance of Liquid-Gas Ejector*. The 9th TSME International Conference on Mechanical Engineering, Phuket, Thailand, December 2018.

[3] Witte, J.H. 1962. *Mixing shocks and their influence on the design of liquid-gas ejectors*, Ph.D. dissertation, Netherlands: TU Delft University.

[4] Witte, J.H. 1969. Mixing shocks in two-phase flow, *Journal Fluid Mechanics*, 36(4), 639-655.

[5] Tang, J., Zhang, Z., Li, L., Wang, J., Liu, J. and Zhou, Y. 2016. Influence of driving fluid properties on the performance of liquid-driving ejector, *International Journal of Heat and Mass Transfer*, 101, 20-26.

[6] Cunningham, R.G. and Dopkin R.J. 1974. Jet breakup and mixing throat lengths for the liquid-jet gas pump, *Journal Fluids Engineering*, 94(3), 216-226.

[7] Yadav, R.L. and Patwardhan, A.W. 2008. Design aspects of ejectors: effects of suction chamber geometry, *Chemical Engineering Science*, 63, 3886-3897.

[8] Kim, I.M., Kim, O.S., Lee, D.H. and Kim, S.D. 2007. Numerical and experimental investigations of gas–liquid dispersion in an ejector, *Chemical Engineering Science*, 62, 7133-7139.

[9] Schindelin, J., Arganda-Carreras, I. and Frise, E. 2012. Fiji: an open-source platform for biological-image analysis, *Nature methods*, 9(7), 676-682.

[10] Schindelin, J., Rueden, C.T., Hiner, M.C. and Eliceiri, K.W. 2015. The imageJ ecosystem: an open platform for biomedical image analysis, *Molecular Reproduction & Development*, 82, 518-529.

[11] Tomczak, L. and Sowinski, J. 2007. Application of image analysis to determine two-phase liquid-gas flow parameter in narrow minichannels, *Chemical and Process Engineering*, 28, 1137-1145.

[12] Wang, H.Y. and Dong, F. 2009. A method for bubble volume calculating in vertical two-phase flow, *Journal of Physics: Conference Series*, 147, 1-12.

[13] Choi, S.H., Ji, H.S. and Kim, K.C. 2015. Comparative study of hydrodynamics with respect to direction of installation of gas-liquid ejector system, *Journal Mechanical Science and Technology*, 29(8), 3267-3276.

[14] Widyatama, A., Dinaryanto, O., Indarto and Deendarlianto. 2018. The development of image processing technique to study the interfacial behavior of air-water slug two-phase flow in horizontal pipes, *Flow Measurement and Instrumentation*, 59, 168-180.

[15] Dibek, B. and Demir H. 2016. Determination of void fraction by image processing, *Uludağ University Journal of The Faculty of Engineering*, 22(3), 97-114.